JOURNAL OF Applied Polymer SCIENCE

Preparation of Highly Dispersed Expanded Graphite/Polypropylene Nanocomposites Via Low Temperature Processing

Mohammad Fasihi,[1] Hamid Garmabi,[1] Seyed Reza Ghaffarian,[1] Masahiro Ohshima[2]

[1]Department of Polymer Engineering and Color Technology, Amirkabir University of Technology, Tehran 15875-4413, Iran

[2]Department of Chemical Engineering, Kyoto University, Kyoto 615-8510, Japan

Correspondence to: H. Garmabi (E-mail: garmabi@aut.ac.ir)

ABSTRACT: A new processing scheme for preparing highly dispersed expanded graphite/polypropylene (PP) nanocomposites has been developed in this study. To improve the degree of dispersion of graphite throughout the PP domains, the solid-state milling has been performed followed by low-temperature melt processing in the range of melting point (T_m) and the crystallization temperature (T_c) of PP. The solid-state milling followed by low-temperature melt mixing could drastically improve the degree of graphite dispersion in the matrix. As a result, the well-dispersed graphite/PP nanocomposite supported by transmission electron microscopy (TEM) exposed a higher degree of plastic deformation and energy to break in the tensile test. The higher degree of graphite dispersion achieved in this scheme was due to the increase of local shear force near the crystalline domains formed during low-temperature melt mixing.
 J. Appl. Polym. Sci. 000: 000–000, 2013

KEYWORDS: nanostructured polymers; morphology; polyolefins; mechanical properties

Received 11 December 2012; accepted 23 February 2013; published online 00 Month 2013
DOI: 10.1002/app.39222

INTRODUCTION

In the recent years, there have been numerous researches focusing on polymeric nanocomposites and showing several promising properties superior to neat polymers even at low-level fractions of fillers.[1–3] The final properties of nanocomposites determined by their structure and nanofiller content. However, achieving the high degree of nanofiller dispersion is still a major challenge in polymeric nanocomposites. Thus, an economic and environment-friendly method of preparing highly dispersed nanocomposites is required in practice.[4–6]

Graphite is a carbon-base material possessing a layered and planar structure. It has been attracting great attention in nanotechnology and known as one of the most suitable materials in terms of mechanical strength and electrical properties.[7] The unique properties and cost-effectiveness of graphite have made it an attractive nanofiller for many purposes.[8,9] In general, graphite/polymer nanocomposites have potential applications in sensors, electromagnetic interference (EMI) shielding, antistatic products, corrosion-resistant coatings, and other functional applications. However, exfoliation of graphite in nanosclae is too difficult via conventional methods. Many researchers have proposed some new methods of mixing or chemical treatments, such as solution-sonication, preparation of graphite oxide, graphite intercalation compound (GIC), expanded graphite (EG) or other functionalization routes to achieve a nano-structured material.[10–15] But chemical treatments usually cause deterioration of graphite properties considerably.

In this work, we employed a simple strategy to prepare expanded graphite/polypropylene nanocomposites representing a well-dispersed morphology using of solid-state milling followed by low-temperature melt mixing. During milling, the particle size of polypropylene was reduced and the breakdown of graphite agglomerates was promoted by solid shear force and the friction between polymer and graphite so that the polypropylene surface particles were completely coated by the graphite. Furthermore, it is known that in semi-crystalline polymers like PP, some crystalline areas are formed up to a point during processing at temperatures above the crystallization temperature, T_c, and under the melting temperature, T_m. We demonstrated that crystallization during mixing in a low-temperature melt condition can significantly improve the degree of exfoliation of graphite in the polypropylene matrix.

EXPERIMENTAL

Materials

Polypropylene (Daploy WB130HMS, Borealis AG) and expandable graphite (EX9980-200N, Beijing Invention Biology Engineering & New Material Co.) were used as received.

Applied Polymer SCIENCE

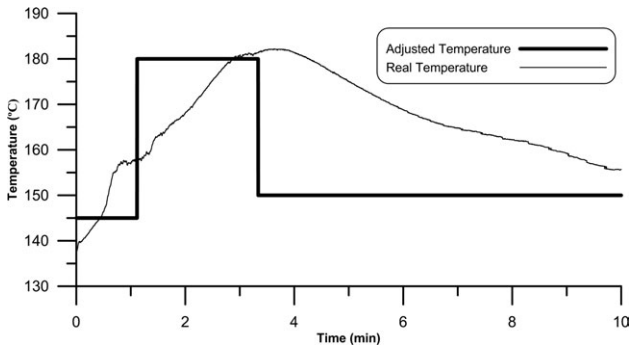

Figure 1. Temperature profile for low-temperature melt-mixing (Scheme A).

Table I. Samples Nomenclature and Mixing Conditions

Samples	Graphite content (wt %)	Preparation scheme
PP	0	Scheme C[low-temp. melt compounding]
PA1	1	Scheme A[180°C melt compounding only]
PB1	1	Scheme B[solid-state milling+ 180°C melt compounding]
PC1	1	Scheme C[solid-state milling+ low-temp. melt compounding]

Sample Preparation

Expandable graphite was prepared through heat shock under 1000°C in an electronic furnace for 30 s. Polypropylene and expanded graphite were mixed together and milled by a freeze-crushing machine (As One TPH-02) for 10 min in the presence of liquid nitrogen. Subsequently, the mixture of PP and graphite powder was melt compounded by a batch melt mixer (Labo-Plastomill 4C150, Toyo Seiki). The rotation speed and processing time were set at 100 rpm and 10 min, respectively.

As illustrated in Figure 1, a temperature programming with three set-points (Scheme C) was arranged to implement compounding. The first set-point temperature was given at 145°C, then the second was raised to 180°C so as to melt PP completely, and the third was at 150°C to increase shear force and friction through cooling. For comparison and to confirm that degradation would not occur in the course of the temperature treatment, neat PP was processed by the melt mixing under the same temperature profile (Scheme C). Furthermore, to see the effect of the melt mixing temperature and solid-state milling on the degree of graphite dispersion, two other preparation schemes were also conducted: in scheme A, expanded graphite and PP were dry-blended and melt-compounded by the melt-mixer without solid-state milling, and in Scheme B, expanded graphite and PP were milled and then melt-compounded at 180°C without applying of compounding at the cooling process.

After the melt compounding, all the samples were compression-molded at 200°C to prepare a 2-mm thick sheet. The samples' nomenclature and their melt mixing condition are listed in Table I.

CHARACTERIZATIONS

Tensile Properties

The tensile tests were carried out using the Autograph (Shimadzu Autographs AGS-J Series) at the ambient temperature with the strain rate of 1 mm/min. The test pieces, 2 mmin thickness, 11 mmin width and 6 mm in length were cut out from the compression-molded samples. Five specimens from each sample were tested.

Morphological Analysis

Transmission electron microscopy (TEM; JEOL JEM-1010) operating under 100 kV was applied to the cryo-microtomed specimens around 70 nm in thickness.

Differential Scanning Calorimetry

The crystallization behavior was observed taking advantage of a differential scanning calorimeter (DSC) (Perkin-Elmer, Pyris 1) under nitrogen atmosphere. The crystallization was measured by heating the sample up to 200°C at a heating rate of 10°C/min to complete melting, then a cooling to 150°C at a cooling rate of 4°C/min and heating again to 200°C at a rate of 10°C/min was emplyoed. This program was selected to estimate the crystallization during low-temperature melt processing. Crystallinity of the sample was calculated from $\Delta H_m/207.1$ ratio, where ΔH_m and 207.1 are enthalpy of melting for partial and 100% crystallinity both in J/g, respectively.

XRD

XRD (MultiFlex, Rigaku Co.) was measured in the range 2θ = 5–30°making use of Ni-filtered Cu/Ka radiation (λ = 0.154 nm) at 40 kV and 20 mA.

Rheological Analysis

The linear viscoelastic behavior of the prepared nanocomposite was measured by ARES mechanical spectrometer (Rheometric Science, USA). The frequency sweep test measurement was conducted with parallel plate geometry (25 mm in diameter with 1.0 mm in gap and 5% strain).

RESULTS AND DISCUSSION

Mechanical Properties of the Samples

Figure 2 displays the photographic images of the composite prepared by each scheme. As observed, graphite was poorly dispersed in PA1 sample prepared via the Scheme A, and agglomeration in the range of hundreds micron length was also observed. The dispersion of graphite was clearly improved in PB1 and PC1. The appearance of PB1 and PC1 was almost the same: their colors were black, and no major difference existed in the photographic level. Figure 2(b) presents the mixture right after solid-state milling. It can be observed that solid-state milling could provide the effective frictional force to graphite and polymer powder so that PP particles were covered with a thin layer of graphite stacks.

The tensile behaviors of the four samples are illustrated in Figure 3. Both PB1 and PC1 showed a slight increase in elasticity. The tensile modulus and tensile strength of neat PP treated by scheme C were 932±63 and 33.4±1.1 MPa, respectively,

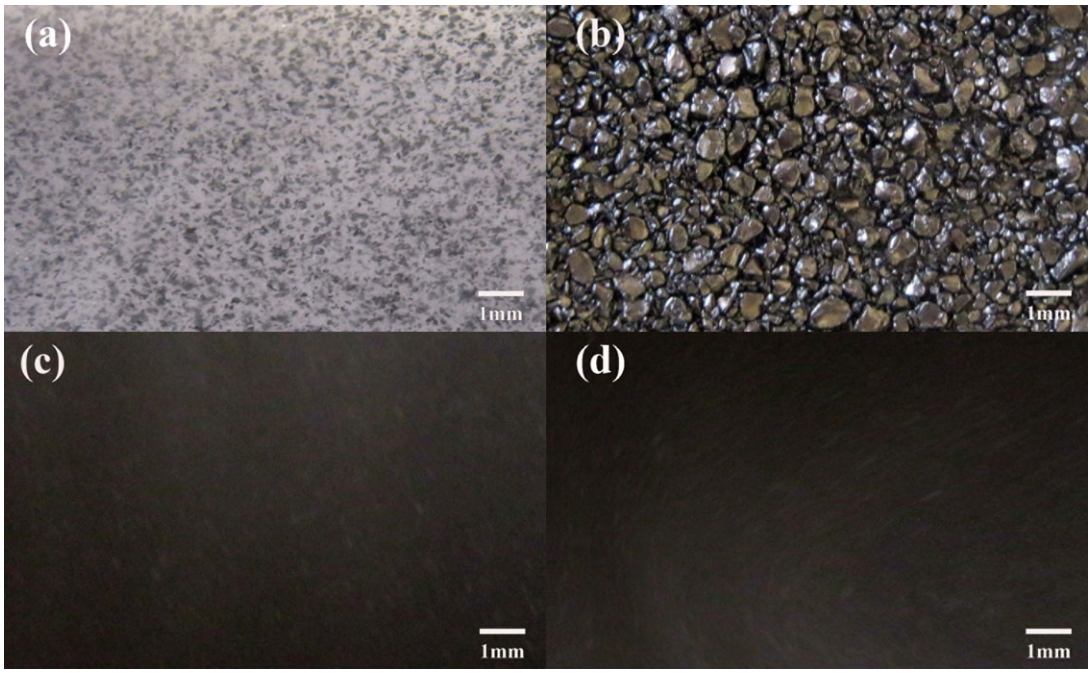

Figure 2. Photographic images of the nanocomposite (a) PA1, (b)PP-coated graphite after solid-state milling,(c) PB1 and (d)PC1. [Color figure can be viewed in the online issue, which is available at wileyonlinelibrary.com.]

which were increased to 1030±58 MPa and 36.1±1.3 MPa for PB1, and 1194±72MPa and 35.3±1.7 MPa for PC1. On the other hand, these properties were decreased to 915±81MPa and 30.2±1.6 MPa in PA1 attributed to the poor dispersion of graphite in the nanocomposite prepared using scheme A. Moreover, the superior plastic deformation of PC1 sample surprisingly led to almost 2-fold (from 12.8±1.1% to 22.6±1.3%) and 3-fold (from 2.1 ± 0.1 J to 5.4 ± 0.1 J) increases in the elongation at break and energy to break, respectively, associated with this sample compared with those of PP sample.

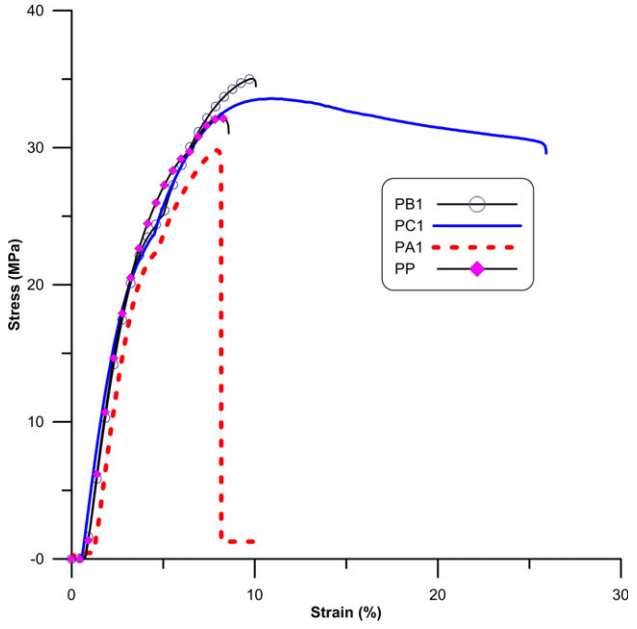

Figure 3. Tensile strain–stress curve of the prepared nanocomposites and neat PP. [Color figure can be viewed in the online issue, which is available at wileyonlinelibrary.com.]

Theoretically, the cohesion force between the graphite layers can be calculated by considering graphite as a multilayer system and applying Lifshitz's formulation of Van der Waals forces. This cohesion force equals to the pressure needed to overcome the binding force between the graphite layers, and is given by[16]:

$$P = \frac{\partial E}{\partial l} = \frac{A_{\mathrm{Ham}}}{6\pi l^3} \tag{1}$$

where E is the free energy of interaction per unit area between the two layers, A_{Ham} is the Hamaker coefficient, and l is the interlayer distance. Taking $A_{\mathrm{Ham}} = 2.3 \times 10^{-19}$ J[17] and $l = 0.335$ nm, the calculated pressure required to separate the two graphite sheets is around 325 MPa. Because the Van der Waals binding force is inversely proportional to l^3, it will be decreased dramatically by increasing the interlayer distance during graphite expansion. On the other hand, owing to the very small distance between graphite layers (around 10 times lower than the radius of polymer entanglement) and also the weak interaction between polypropylene and graphite, diffusion of polymer chains between the graphite layers will be impossible, and graphite layers should be separated by peeling force applied within melt mixing. The shear stress generated during melt mixing can be obtained by:

$$\tau = \eta(\dot{\gamma})\,\dot{\gamma} \tag{2}$$

The maximum shear rate during mixing in the batch mixer is given by[18]:

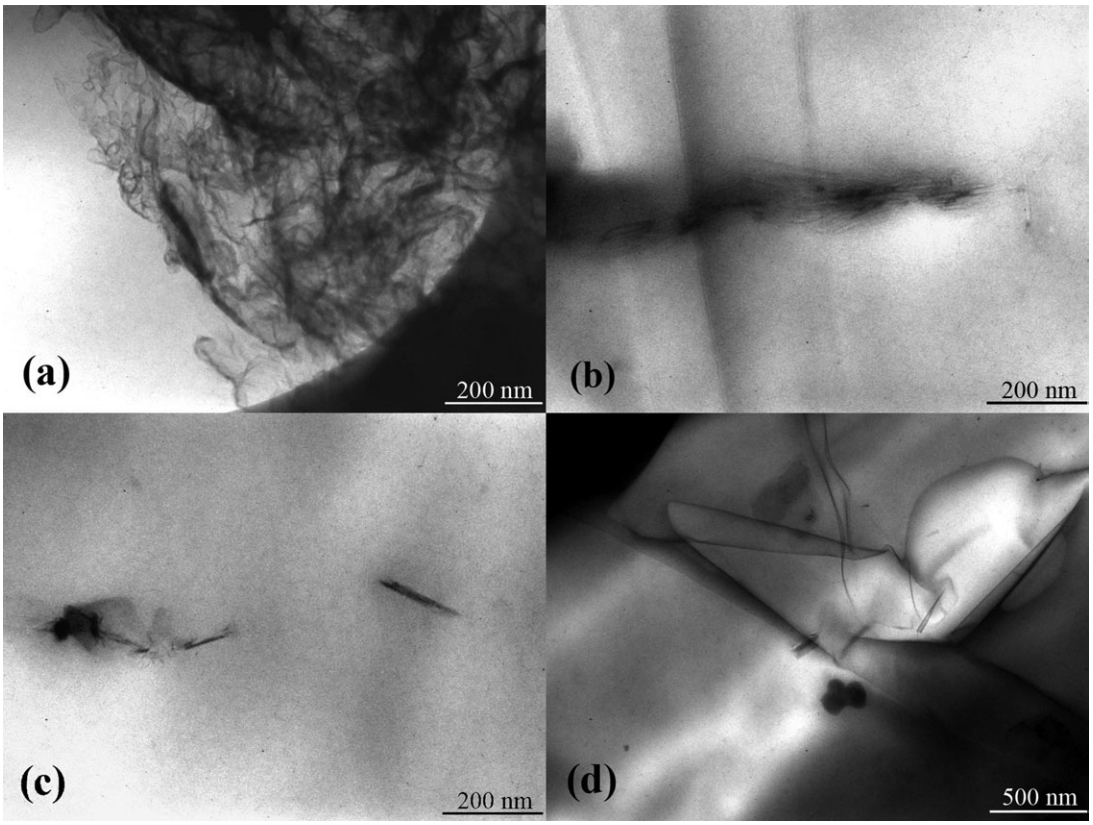

Figure 4. Transmission electron micrograph of (a) PA1, (b) PB1, and (c,d) PC1.

$$\gamma_{\max} = \frac{4\pi N}{n} \frac{\left(\frac{R_e}{R_i}\right)^{2/n}}{\left(\frac{R_e}{R_i}\right)^{2/n} - 1} \quad (3)$$

where R_e, R_i, N, and n are outer radius, inner radius, rotational speed, and power law index of the polymer, respectively. By applying $n = 0.46$ for PP, $N = 100$ rpm and $R_e/R_i = 1.083$ and considering the viscosity at the calculated shear rate, the maximum-achieved shear stress is smaller than 0.55 MPa, almost three orders of magnitude lower than the pressure needed to overcome the cohesion force between the graphite layers. Due to the shear thinning behavior of polymers, the shear stress cannot be increased effectively by increasing the shear rate. The predicted rotational speed to obtain the binding force of graphite will be bigger than 10^8 rpm, which is not achievable through any conventional melt mixing devices. Therefore, we can conclude that it is almost impossible to get exfoliated or intercalated morphology in graphite/polymer nanocomposites using only melt mixing method. From eq. (1) it can be perceived that for exfoliation of graphite during melt mixing, the distance between the graphite layers should be increased at least 10 times, by any treatment or thermal expansion, until the cohesion force of graphite layers decreases as much as three orders, and is placed in the order of the shear stress applied by the melt mixing apparatus. Another way to overcome the binding force between the graphite layers and obtain exfoliated morphology without graphite treatment is an increment of shear stress through increase in the matrix viscosity up to three orders of magnitude [eq. (2)] which is achievable only by implementation of mixing in the solid-state.

Morphological Analysis

Figure 4(a) depicts the TEM image of PA1. The large aggregation of graphite is observed in the sample prepared only through melt-mixing at 180°C. By performing solid-state milling prior to melt mixing, the large aggregates were broken down to tactoids composed of several layers, as illustrated in Figure 4(b). The thickness of the tactoids was around 100 nm. As displayed in Figure 4(c), when the nanocomposite was prepared by conducting solid-state milling and melt compounding at a lower temperature, the graphite was well-dispersed in such a way that the thickness of the tactoids was reduced to values smaller than 20 nm.

The XRD patterns of PP, PB1, and PC1 are shown in Figure 5. Seven peaks corresponding to the α-form crystals were observed in the XRD pattern of PP. An additional peak was detected at $2\theta = 26.6^o$ for PB1 and PC1, which was related to the graphite's plane. The intensity attributed to crystal peaks of PB1 is similar to those of the neat PP. PC1 showed the strongest crystal peaks at $2\theta = 16.9^o$ and $2\theta = 25^o$, which corresponded to $\alpha < 040 >$ and $\alpha < 060 >$ planes, respectively, and matched the crystallographic plane of graphite.[19] Similar results have been observed for exfoliated nanoplatelet graphite (XGnP) reinforced PP, in which the XGnP consists of a few layers of graphene. It has

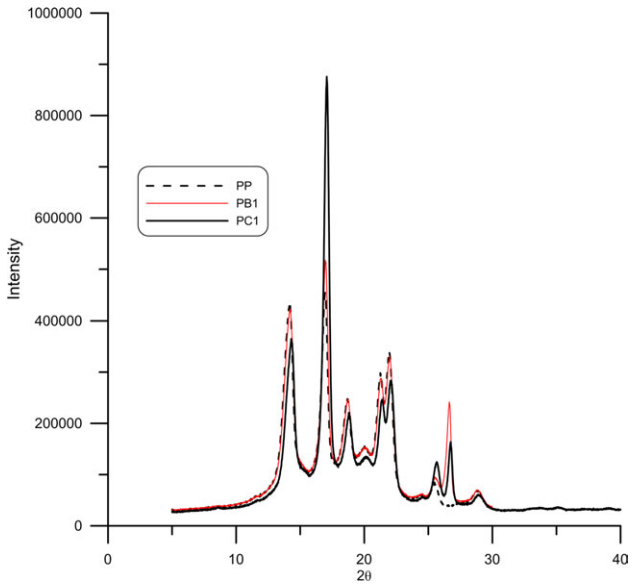

Figure 5. XRD of samples prepared by different mixing method. [Color figure can be viewed in the online issue, which is available at wileyonline library.com.]

been reported that highly dispersed graphite (XGnP) can reinforce the crystal peaks at $2\theta = 16.9^{o}$ and $2\theta = 25^{o}$, which matched the crystallographic plane of graphite.[19] Besides, although the graphite plane peak at $2\theta = 26.6^{o}$ did not disappear completely in PC1, the intensity of those peaks was reduced to about half of those of PB1. These results, supported by TEM images, revealed the higher degree of exfoliation of PC1 and the better quality of mixing achieved by solid-state milling followed by low-temperature melt compounding.

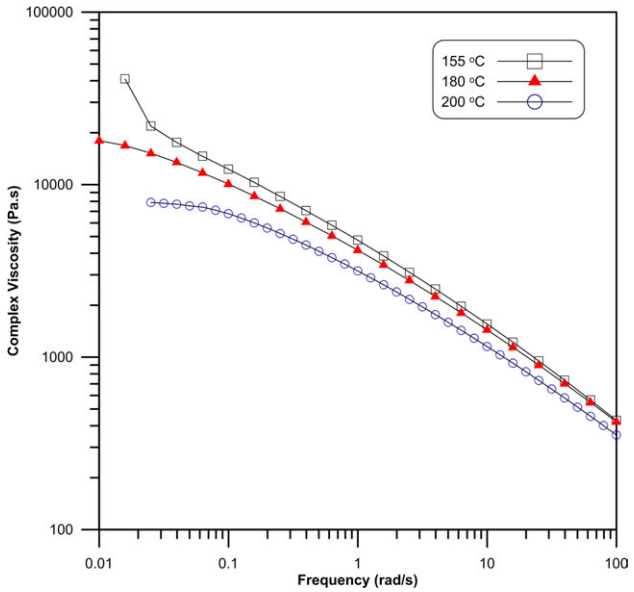

Figure 6. Complex viscosity of PP at different temperature. [Color figure can be viewed in the online issue, which is available at wileyonline library.com.]

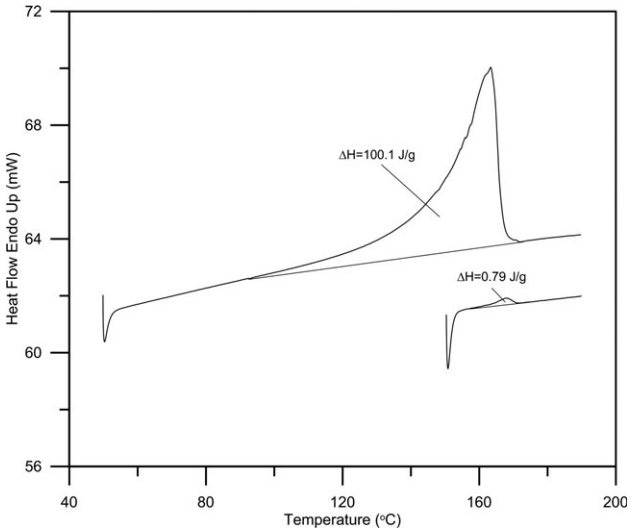

Figure 7. Enthalpy of melting for PC1 by heating from room temperature (above) and from 150°C after melting and cooling program (below).

Rheological Analysis

Melt viscosity of polypropylene has low sensitivity to temperature. Figure 6 presents the complex viscosity of PP at three different temperatures. The viscosities at 155 and 180°C, the two processing temperatures, are almost the same at most of the shear rate ranges. Only at very low shear rates, the viscosity increased at 155°C. This upturn in viscosity could be attributed to the existence of crystals in the polypropylene matrix at this temperature. During melt mixing of the samples, shear rate in different areas of the batch mixer varied between 600 – 3000 s^{-1}.[18] It means that in this mixing conditions, the viscosity of polypropylene matrix cannot be responsible for the big difference in the mixing quality of the samples processed at a high temperature (PB1) and a low temperature (PC1).

To infer the presence of crystals during low-temperature melt compounding, the crystallinity was measured by DSC at a temperature profile similar to the processing condition (Scheme C). The melting temperature for all the samples measured by DSC was 163.0±1.0°C. The results of DSC shown in Figure 7 revealed that around 0.38 wt % crystal was formed in the polypropylene media treated by Scheme C. As many researchers have reported the shear-induced crystallization of PP,[20–22] could be perceived that the higher shear rate induced the higher rate of crystallization and changed the crystal structure. However, accurate measurement of crystallinity under specified shear rate is difficult and the exact relationship between crystallinity and the measurable process variables has not been reported yet. As an estimate, we used the Einstein relation for dilute solution:

$$\frac{T_{PF1}}{T_{PB1}} \approx \frac{\tau_{PF1}}{\tau_{PB1}} \approx \frac{\eta_{PF1}}{\eta_{PB1}} \tag{4}$$

$$\frac{\eta_{PF1}}{\eta_{PB1}} = (1 + 2.5\phi) \tag{5}$$

where T, τ, η, and φ stand for the applied torque by mixing machine, shear stress, viscosity during processing and volume

Applied Polymer SCIENCE

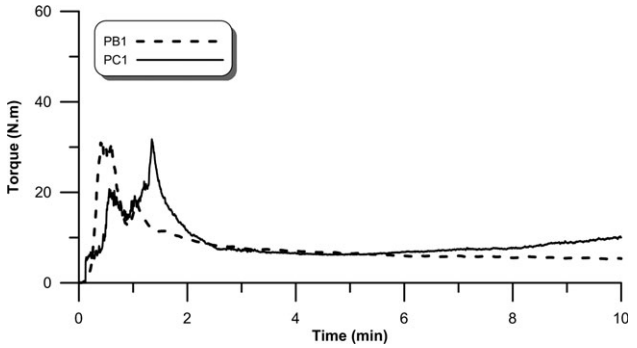

Figure 8. The torque recorded by the batch mixer during compounding for PB1 and PC1.

fraction of the filler, respectively. Regarding crystals as a filler with the assumption that the upturn at the end of the torque curve (Figure 8) was caused by crystallization of the polymer, φ was calculated to be 0.57. The amount of crystals was not high enough to cause large changes in the total viscosity of PP. It represents just a small upturn at the end of the torque-time curve (Figure 8), but the low amount of crystals changed the homogeneous molten PP media to heterogeneous media consisting of solid particles (crystals). Existence of these crystals could increase the local shear force near the crystalline domain, which is transferred to graphite particles. As a result, exfoliation of graphite layers could be advanced up to higher levels.

CONCLUSIONS

This study demonstrated the potential of solid-state milling followed by low-temperature melt compounding for preparation of a well-dispersed expanded graphite/polypropylene nanocomposite. The well-dispersed graphite/PP nanocomposites revealed a higher degree of plastic deformation and energy to break in the tensile test; moreover, showed higher degree of exfoliation in TEM images. The better dispersion at low temperature melt mixing was attributed to formation of a small fraction of crystal particles, which built up the heterogeneity of the media and increased the local shear force near the crystal particles.

REFERENCES

1. Jordana, J.; Jacobb, K. I.; Tannenbaumc, R.; Sharaf, M. A.; Jasiuk, I. *Mater. Sci. Eng. A* **2005**, *393*, 1.
2. Sheng, N.; Boyce, M. C.; Parks, D. M.; Rutledge, G. C.; Abes, J. I.; Cohen, R. E. *Polymer* **2004**, *45*, 487.
3. Tjong, S. C. *Mater. Sci. Eng. R* **2006**, *53*, 73.
4. Du, Y.; Shen, S. Z.; Cai, K.; Casey, P. S. *Prog. Polym. Sci.* **2012**, *37*, 820.
5. Emmanuel, P.; Giannelis, P. *Adv. Mater.* **1996**, *8*, 29.
6. Schadler, L. *Nat. Mater.* **2007**, *6*, 257.
7. Setton, R.; Bernier, P.; Lefrant, S. Carbon Molecules and Materials; Taylor & Francis: London, **2002**.
8. Geim, A. K.; Novoselov, K. S. *Nat. Mater.* **2007**, *6*, 183.
9. Flandin, L.; Cavaillé, J. Y.; Bidan, G.; Brechet, Y. *Polym. Comp.* **2000**, *21*, 165.
10. Persson, H.; Yao, Y.; Klement, U.; Rychwalski, R. W. A. *Express Polym. Lett.* **2012**, *6*, 142.
11. Dresselhaus, M. S.; Dresselhaus, G. *Adv. Phys.* **2002**, *51*, 1.
12. Kim, H.; Abdala, A. A.; Macosko, C. W. *Macromolecules* **2010**, *43*, 6515.
13. Stankovich, S.; Dikin, D. A.; Piner, R. D.; Kohlhaas, K. A.; Kleinhammes, A.; Jia, Y.; Wu, Y.; Nguyen, S. T.; Ruoff, R. S. *Carbon* **2007**, *45*, 1558.
14. Potts, J. R.; Dreyer, D. R.; Bielawski, C. W.; Ruoff, R. S. *Polymer* **2011**, *52*, 5.
15. Wakabayashi, K.; Pierre, C.; Dikin, D. A.; Ruoff, R. S.; Ramanathan, T.; Brinson, L. C.; Torkelson, J. M. *Macromolecules* **2008**, *41*, 1905.
16. Parsegian, V. A. van der Waals Forces: A Handbook for Biologists, Chemists, Engineers, and Physicists, Cambridge University Press: Cambridge, **2005**.
17. Visser, J. *Adv. Colloid Interface Sci.* **1972**, *3*, 331.
18. Bousmina, M.; Ait-Kadi, A.; Faisant, J. B. *J. Rheol.* **1999**, *43*, 415.
19. Kalaitzidou, K.; Fukushima, H.; Askeland, P.; Drzal, L.T. *J. Mater. Sci.* **2008**, *43*, 2895.
20. Xu, J. Z.; Chen, C.; Wang, Y.; Tang, H.; Li, Z. M.; Hsiao, B. S. *Macromolecules* **2011**, *44*, 2808.
21. D'Haese, M.; Puyvelde, P. V.; Langouche, F. *Macromolecules* **2010**, *43*, 2933.
22. Yu, F.; Zhang, H.; Liao, R.; Zheng, H.; Yu, W.; Zhou, C. *Euro. Polym. J.* **2009**, *45*, 2110.